Fullerenol–Cytotoxic Conjugates for Cancer Chemotherapy

Padmaparna Chaudhuri[†,‡] Abhimanyu Paraskar,[⊥,†,‡] Shivani Soni[⊥,†,‡] Raghunath A. Mashelkar[†,§] Shiladitya Sengupta[†,‡,*]

[†]Laboratory of Nanomedicine, HST Center for Biomedical Engineering, Department of Medicine, Brigham and Women's Hospital, [‡]Harvard–MIT Division of Health Sciences and Technology, Harvard Medical School, and [§]National Chemical Laboratories, Pune, India. [⊥]These authors contributed equally to this study.

ABSTRACT In the present study, we report the novel application of polyhydroxylated fullerenes (fullerenols) in cancer drug delivery. The facile synthetic procedure for generating multiple hydroxyl groups on the fullerene cage offers scope for high drug loading in addition to conferring hydrophilicity. Doxorubicin, a first line cancer chemotherapeutic, was conjugated to fullerenols through a carbamate linker, achieving ultrahigh loading efficiency. The drug–fullerenol conjugate was found to be relatively stable in phosphate buffer saline but temporally released the active drug when incubated with tumor cell lysate. The fullerenol–doxorubicin conjugate suppressed the proliferation of cancer cell-lines *in vitro* through a G2-M cell cycle block, resulting in apoptosis. Furthermore, in an *in vivo* murine tumor model, fullerenol–doxorubicin exhibited comparable antitumor efficacy as free drug without the systemic toxicity of free doxorubicin. Additionally, we demonstrate that the fullerenol platform can be extended to other chemotherapeutic agents, such as the slightly water-soluble cisplatin, and can emerge as a new paradigm in the management of cancer.

KEYWORDS: fullerenol · nanoparticle · chemotherapy · doxorubicin · drug delivery

Nanotechnology has been recognized by the National Cancer Institute as a paradigm-changing opportunity with the potential to enable significant breakthroughs in cancer diagnosis and therapy.[1] The promise of cancer nanotechnology lies in the ability to engineer customizable nanoscale constructs that can be loaded with one or more payloads such as chemotherapeutics, imaging, and diagnostic agents.[2] However, nanocarriers widely explored to date such as liposomes,[3] polymers,[4] and dendrimers[5] suffer from inherent limitations such as instability, structural heterogeneity, synthetic challenges, and poor control over shape and size. Hence, there is an increasing need for advanced delivery agents where shape, size distribution, functionalization, and loading capacity can be precisely tuned, with the assumption that a greater control over the physical parameters of the nanodevices may allow tunability of their biological fate.[6]

The potential of fullerene to address the above design specifications lies in the immense scope for chemical derivatization to the basic structure.[7] In recent years, carbon nanotechnology has evolved into a truly interdisciplinary field, bridging material science with medicine. However, among the various currently available carbon nanomaterials, it is the carbon nanotube (CNT), which has been mainly explored for biomedical applications such as in the delivery of drugs or as probes for imaging.[8,9] In contrast, fullerenes, the third allotrope of carbon after diamond and graphite, have had limited use in biology due to their inherent hydrophobicity. The recent discovery that water-soluble fullerene derivatives can cross cell membranes[10] has accelerated interest in biological applications of C_{60}[11–16] such as in gene delivery.[12] Endohedral metallofullerenes have demonstrated potential as radiopharmaceuticals[17] and MRI contrast agents.[18] However, the application of fullerenes as carriers of chemotherapeutics is still in a very nascent stage. There are only a few reports in the literature where fullerene derivatives have been used for the delivery of anticancer therapeutics.[19,20] Recently, an amphiphilic fullerene (buckysome) was explored as a vector for paclitaxel and was found to be equiefficaceous to Abraxane, a commercially available albumin-bound nanoformulation of paclitaxel.[21]

In the present study, we explored the novel application of polyhydroxylated fullerene (fullerenol) in drug delivery. The high aqueous solubility, neutral pH of fullerenols, and accessibility to further modification makes them promising candidates for medical applications.[22] Additionally, the facile synthetic procedure to produce multiple hydroxyl groups[22] offers scope for high drug loading. We demonstrate that the fullerenols enable the

*Address correspondence to shiladit@MIT.edu.

Received for review March 30, 2009 and accepted August 07, 2009.

Published online August 14, 2009.
10.1021/nn900318y CCC: $40.75

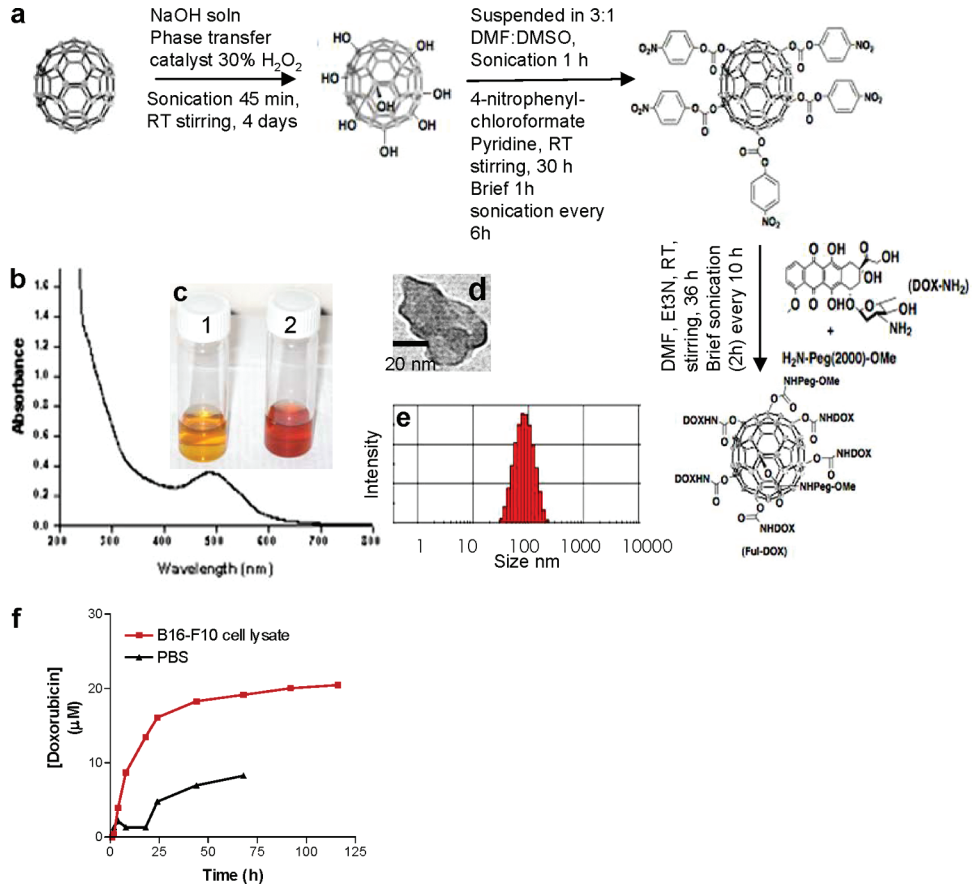

Figure 1. Synthesis and characterization of doxorubicin conjugated fullerene nanoparticle: (a) schematic illustration of the synthetic steps for fullerene functionalization and conjugation of doxorubicin; (b) UV−absorption spectra of the nanoparticle-drug conjugate solution in water showing the doxorubicin absorption at 490 nm; (c) solution of (1) fullerenol and (2) Ful−Dox in water. Transmission electron microscopy shows a (d) magnified image of a single fullerene aggregate at 60K magnification, (e) Dynamic light scattering analysis of the nanoparticle-drug conjugate aggregate showing an average size distribution around 80 nm; (f) graph shows the temporal release kinetics of doxorubicin from fullerenol in tumor cell lysate and in phosphate buffered saline (PBS, pH 7.4). Concentrated drug-loaded nanoparticles were suspended in tumor cell lysate or PBS and dialyzed against buffer. An aliquot was collected from the incubation medium at predetermined time intervals, and the released drug was quantified by absorption spectroscopy at 485 nm wavelength. Data shown are from a representative experiment.

conjugation of high levels of the chemotherapeutic agent, doxorubicin (Dox), which is released in a sustained manner under conditions mimicking tumor pathophysiology. Furthermore, we demonstrate that the susceptibility of tumor cells to nanoparticle-conjugated therapeutics is dependent on the rate of nanoparticle internalization, which can vary between cell types. Treatment with fullerenol−doxorubicin (Ful−Dox) exerted an equi-efficaceous antitumor outcome as compared to free doxorubicin, without the systemic toxicity associated with the latter. Additionally, we demonstrate that the fullerenols can be adapted to formulate the slightly water-soluble cisplatin, which is a first line chemotherapeutic for many cancer types. Our findings demonstrate that the fullerenols could emerge as a versatile platform for delivery of anticancer agents.

RESULTS AND DISCUSSION

Preparation and Characterization of Fullerenol Doxorubicin Nanoparticle. We chose an established procedure, which generates between 16−24 hydroxyl groups on the fullerene cage.[22] Doxorubicin, a potent first line cytotoxic chemotherapy, was selected as the active agent. The pegylated Ful−Dox conjugate was synthesized as outlined in Figure 1a. Briefly, to a deep purple toluene solution of fullerene, NaOH solution was added along with a few drops of 30% hydrogen peroxide and a phase transfer catalyst. After 5 days the colored aqueous layer was separated from the colorless organic layer and product was precipitated out with ethanol. The resulting brown solid showed a broad OH stretching frequency at 3400 cm^{-1} in FTIR and was completely water-soluble. The hydroxyl groups of fullerenol were activated by reaction with *p*-nitrophenylchloroformate. The attachment of the nitrophenyl group was confirmed by NMR peaks at 6.9 and 8.2 ppm. The activated fullerenol was then conjugated to doxorubicin and OMe-Peg(2000)-NH_2 by simultaneous addition of the two reagents in a 2:1 molar ratio. While we anticipated each fullerenol particle to be no greater than 5 nm following pegylation and conjugation of doxorubicin, we observed that the fullerenols tend to form mon-

odisperse aggregates in the size range of 50−80 nm as confirmed by dynamic laser light scattering and electron microscopy (Figure 1d,e). These could not be disintegrated into smaller individual fullerenols and could arise from intermolecular interactions, such as H-bonding. However, the particle sizes were uniformly less than 100 nm, which is an interesting observation from a pharmacokinetic standpoint as nanoparticles less than 5 nm have been reported to be cleared by the kidney,[23] while larger pegylated nanoparticles that are less than 100 nm have been reported to preferentially home into tumors through leaky tumor neovasculature as a result of the enhanced permeability and retention (EPR) effect.[23] While it is beyond the scope of this study to explore the correlation between size and biodistribution of individual fullerenols or the monodisperse aggregates, the tunability of final size opens up the possibility of targeting tumors without being cleared rapidly by the kidney.

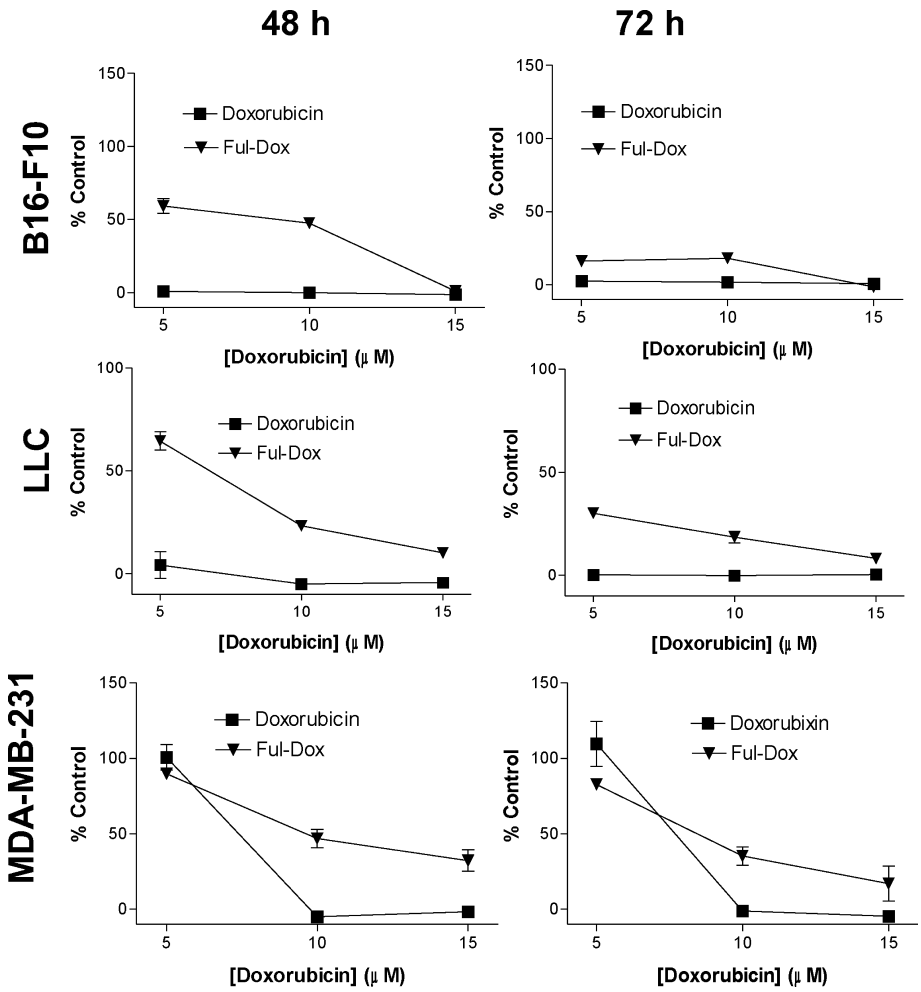

Figure 2. ***In vitro*** **antitumor efficacy of Ful−Dox. Graphs show doxorubicin concentration response on cell survival after treatment with free doxorubicin and Ful−Dox for 48 and 72 h. Mouse melanoma cell line B16−F10, mouse lung carcinoma (LLC1), and metastatic human breast cancer cell line MDA-MB-231 were grown in 96-well plates, with 2000 cells seeded into each well. Drugs were added at appropriate concentrations (5, 10, 15 μM doxorubicin concentration). Cells viability at the experimental time points was quantified using MTS assay. Absorbance of the bioreduced soluble formazan product was measured at 490 nm using a Versamax microplate reader. Results were quantified by subtracting the blank value from each value then normalizing against the control values. Data shown are mean ± SE from $n = 3$.**

Doxorubicin loading to the carbon nanostructures was quantified by absorption spectroscopy at $\lambda_{max} = 485$ nm using the doxorubicin molar extinction coefficient 11500 M^{-1} cm^{-1}, and was found to be between 200−250 μg/mg of the total nanoparticle weight for fullerenes. In contrast, maximal doxorubicin loading in polymeric nanoparticles such as those engineered from PLGA rarely exceeds a third of that. To study the release kinetics of the active drug from the nanoparticle−drug conjugates, we incubated the nanostructures in phosphate buffer saline (pH 7.4) or with cancer cell lysates. As seen in Figure 1f doxorubicin release from the fullerenols had an early onset and was sustained over 100 h. In contrast, the hydrolysis rate was very slow in phosphate buffered saline indicating that intracellular enzymatic processing plays a critical role in the release of the active drug.

In Vitro **Cell Viability of Tumor Cells Treated with Ful−Dox Nanoparticle.** We next tested the efficacy of the drug−nanoparticle conjugates on an array of cancer cell lines. Temporal concentration−response was monitored using an MTS assay (Figure 2). At 24 h, the IC_{50} values of the Ful−Dox conjugate against melanoma and LLC cells was 12 and 10 μM (expressed as doxorubicin concentration), respectively. The cytotoxicity of the drug−nanoparticle conjugates increased with time; that is, the IC_{50} value shifted to the left on the concentration−effect plot, consistent with the slow cleavage of the carbamate bond resulting in sustained release of active doxorubicin. The fullerenols alone had minimal cytotoxicity except at the highest concentrations (Supporting Information, Figure 1). The conjugate was however less efficacious against MDA-MB-231 with an $IC_{50} \approx 8$ μM even after 72 h treatment.

Cellular Uptake of FITC-Labeled Nanoparticles. To further explore this difference in susceptibility of MDA-MB-231 and the B16/F10 cells to the drug−nanostructure conjugates, we studied the uptake of the nanoparticles by the cells (Figure 3). We labeled the fullerenols with FITC, and tracked its internalization into the cells and into the lysosomes through colocalization of the FITC-signal (green fluorescence) with Lysotracker Red (red fluores-

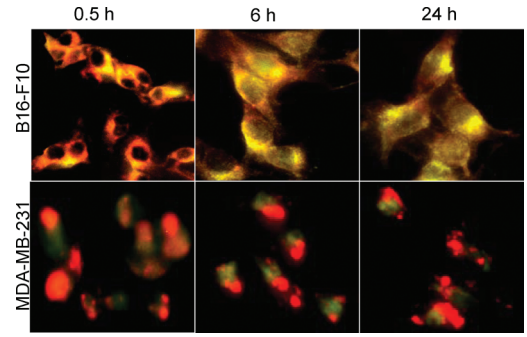

Figure 3. Temporal uptake of FITC-labeled fullerenols into melanoma and breast cancer cells. B16/F10 melanoma and MDA-MB-231 cells were seeded on glass coverslips in 24-well plates at a concentration of 50 000 cells per well. When cells reached ~70% confluency, they were treated with fluorescein isothiocyanate (FITC) labeled carbon nanoparticles for different durations. For colocalization studies, at indicated time points, the cells were washed with PBS and incubated with Lysotracker Red, which is a lysosomal marker. Representative images shown were obtained using a Nikon Eclipse TE2000 fluorescence microscope equipped with green and red filters for FITC and Lysotracker Red, respectively.

cence). The fullerenols showed localization within the lysosomal compartment within 2 h time point in the B16−F10 melanoma cells. In contrast, no internalization was evident even after 2 h in MDA-MB-231 cells and was less compared to melanoma cells at later time points. This is evident in Figure 3, where FITC and Lysotracker fluorescences do not merge in the MDA-MB-231 cell line even after 24 h, indicating low internalization. This distinction in the uptake and hence decreased intracellular processing could explain the difference in susceptibility of the two cell lines to the nanoparticle−drug conjugates. Indeed in a separate study, we observed that polymeric nanoparticles synthesized from polylactic polyglycolic acid copolymers are similarly not internalized into the MDA-MB-231 cells and had limited biological activity.[24]

FACS Analysis of Cell-Cycle Arrest and Apoptosis Induced by Ful−Dox Conjugate. To evaluate the mechanisms underlying the reduction in cell viability following treatment with the drug−nanostructure conjugates, we monitored the effect of treatment on cell cycle (Figure 4), as quantified by measuring the amount of PI-labeled DNA in B16−F10 cells. Following treatment with free doxorubicin for 24 h, majority of gated cells were found to be in the S-phase, 34.2 ± 0.9%, in contrast to 16.6 ± 0.5% in the PBS treated cells, while Ful−Dox induced significant arrest of tumor cells in G2/M phase of the cell cycle (31.4 ± 1.2%, in contrast to 14.6 ± 0.6% in the control). To test whether the inhibition of cell cycle by Ful−Dox conjugates induce apoptosis, we probed the drug-treated cancer cells with annexin-V, which binds to the externalized phosphatidylserine on the surface of apoptotic cells. Counterstaining the cells with propidium iodide enables the distinction between necrotic and apoptotic cells (Figure 5). Indeed, we observed that >99% of the gated melanoma cell population was in late-apoptotic stage following treatment with the nanostructure−conjugated drug for 24 h (Figure 5). Interestingly, in MDA-MB-231 cell line while treatment with free doxorubicin resulted in >99% of the cells shifting to late apoptosis, Ful−Dox had lesser effect

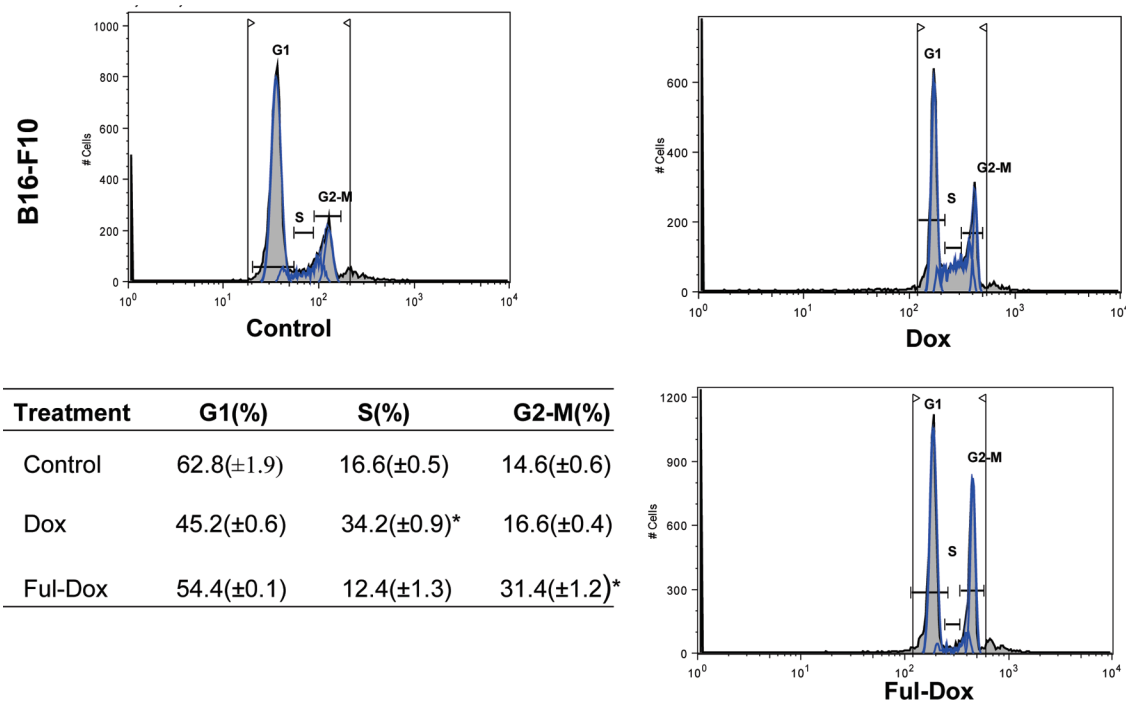

Treatment	G1(%)	S(%)	G2-M(%)
Control	62.8(±1.9)	16.6(±0.5)	14.6(±0.6)
Dox	45.2(±0.6)	34.2(±0.9)*	16.6(±0.4)
Ful-Dox	54.4(±0.1)	12.4(±1.3)	31.4(±1.2)*

Figure 4. Effect of Ful−Dox treatment on cell cycle. Cell-cycle arrest following treatment with free doxorubicin or Ful−Dox was quantified by flow cytometry analysis of propidium iodide-labeled melanoma cells following 24 h of treatment. The average population of cells in each phase of cell cycle are shown in the bar graph. Data shown are mean ± SE from $n = 3$. (*) $P < 0.01$ *vs* vehicle treated control.

with only 31.1 ± 1.7% and 46.2 ± 1.8% cells in early and late-apoptotic stages, respectively. This was consistent with the limited antiproliferative activity seen with the Ful−Dox conjugate in the MDA-MB-231 cells, and can be explained based on the reduced uptake and lysosomal processing of the Ful−Dox conjugates into these cells as compared with B16/F10 cells. Our results indicate that further optimization of the nanoparticles with internalizing peptides or antibodies will be required for targeting cancer cells that exhibit limited internalization of nanoparticles. For example, Ruoslahti *et al*. have demonstrated that an iRGD peptide can not only target tumor *in vivo* but is also internalized,[25] and can be used for active targeting of nanoparticles to tumors.

***In Vivo* Efficacy of Ful−Dox Nanoparticle in a Melanoma-Tumor Model.** To validate the therapeutic efficacy of Ful−Dox conjugate treatment, we randomly sorted mice bearing established B16/F10 melanomas into three groups and treated each group with three injections of (i) free doxorubicin (6 mg/kg), (ii) Ful−Dox (equivalent to 6 mg/kg of doxorubicin dose), or (iii) phosphate buffer saline (PBS, vehicle control). The mice injected with PBS formed large tumors by day 16 (day after the last injection), and were euthanized. The animals in the other groups were also sacrificed at the same time point to evaluate the effect of the treatments on tumor pathology. As shown in Figure 6a, treatment with free doxorubicin or Ful−Dox resulted in a dramatic and similar levels tumor growth inhibition. However, at the dose used, free doxorubicin resulted in a significant decrease in body weight of the animals over the experimental period, while in the nanoparticle−drug conjugate-treated mice we observed an overall gain in body weight (Figure 6b). These results indicate that the conjugation of doxorubicin to the fullerenols increases the therapeutic index of the cytotoxic agent. This could arise from the high water solubility of pegylated fullerenol, which can confer long blood circulation times by reducing nonspecific protein absorption and clearance by the reticuloendothelial system. Furthermore, the nanoconstructs can expectedly accumulate in the tumor tissues (by escaping through the abnormally leaky tumor blood vessels), where enzymatic release of the active drug, mediated by carboxylesterases (that have been shown to be expressed in several tumors including melanoma[26]) can result in focal build-up of the active agent within the tumor resulting in reduced systemic toxic side effect of doxorubicin.[27]

To test this further, we studied the tissue distribution of free doxorubicin and Ful−Dox conjugate. As a positive control, we also included an additional group of animals that received an equivalent dose of doxorubicin conjugated to pegylated single-walled carbon nanotubes (CNT−Dox), which has been extensively characterized *in vivo*.[8] Synthesis of single-walled CNT−doxorubicin conjugate is described in Supporting Information. The level of doxorubicin in lung, heart,

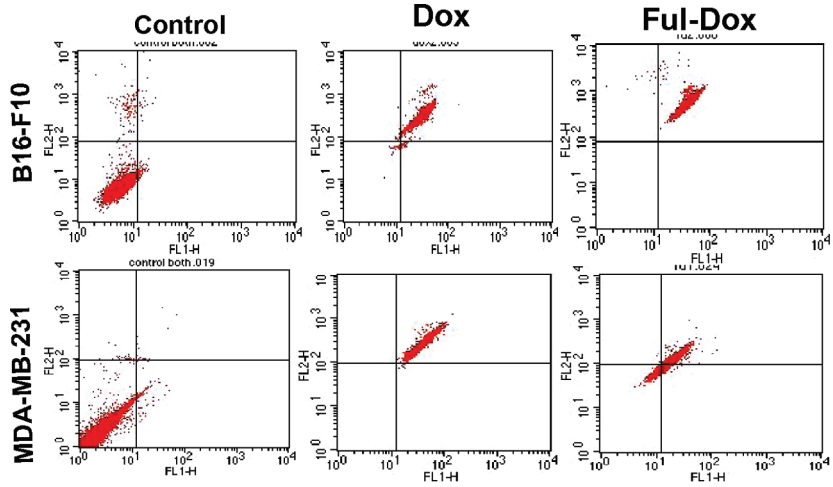

Treatment	Quadrant Statistics (B16-F10)			
	UL	UR	LR	LL
Control	1.1 (0.1)	0.2(0.04)	0.8(0.1)	97.8(2.0)
Dox	0.7(0.5)	97.0(3.0)*	0.9(0.9)	1.6(2.1)*
Ful-Dox	0.3(0.2)	99.7(0.2)*	0.01(0.01)	0.03(0.01)*

Treatment	Quadrant Statistics (MDA-MB-231)			
	UL	UR	LR	LL
Control	1.1 (0.03)	0.6(0.6)	0.8(0.1)	98.9(0.2)
Dox	0	99.8(0.4)*	0.2(0.04)	0
Ful-Dox	0.1(0.1)	46.2(1.8)*	31.1(1.7)*	22.3(3.1)*

Figure 5. Induction of apoptosis in cells treated with Ful−Dox. The effect of free doxorubicin (Dox) or Ful−Dox on the induction of apoptosis in tumor cells, after 24 h treatment, was quantified by flow cytometry analysis of AnnexinV−Alexa488 stained melanoma and breast cancer cells. The cells were counterstained with propidium iodide. The lower left (LL) quadrant represents live/healthy cells, the lower right (LR) quadrant represents early apoptosis, the upper right (UR) represents cells in late apoptosis, while the upper left (UL) represents necrotic cells. In the table, the average percentage of the total gated cell population in each of the quadrants are shown. Data shown are mean ± SE (shown in parentheses) of $n = 3$. (*) $P < 0.001$ *vs* vehicle treated control. (ANOVA followed by Newman-Keuls test).

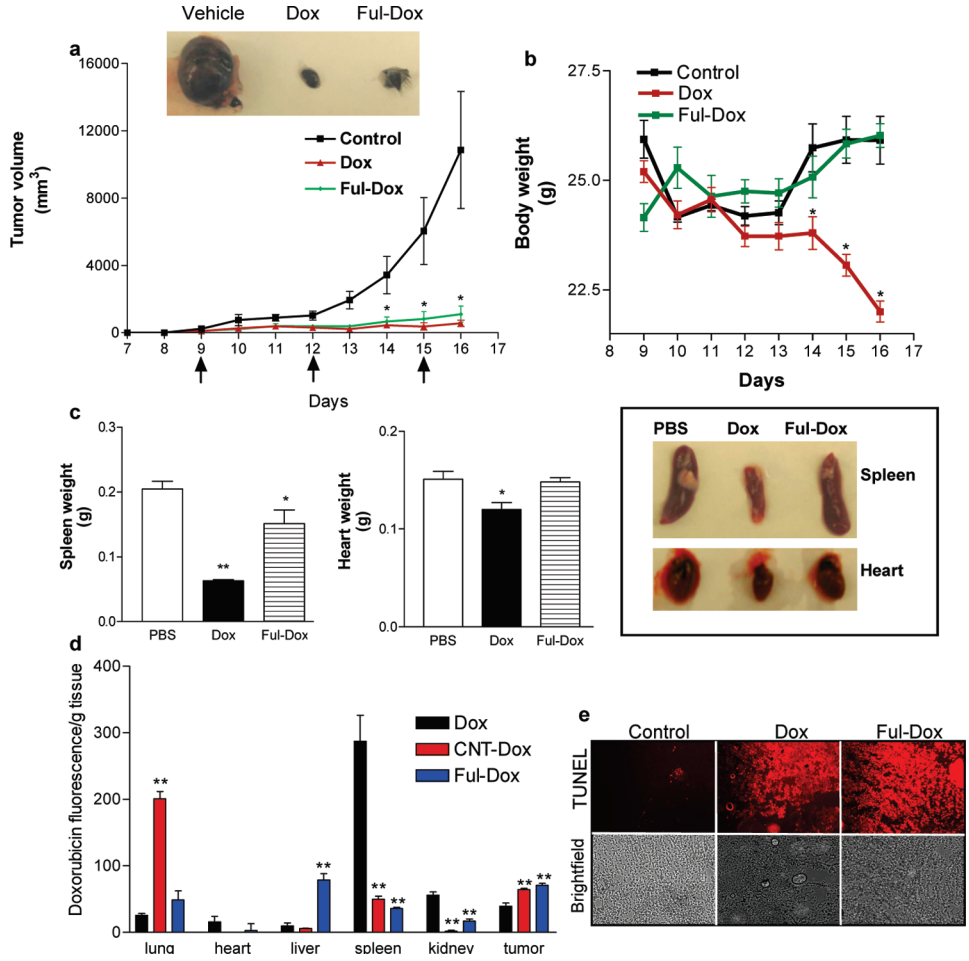

Figure 6. ***In vivo*** **efficacy of nanoparticle−drug conjugates studies in a mice melanoma tumor model. Melanoma bearing animals were injected with three doses of doxorubicin or carbon nanostructure conjugated doxorubicin equivalent to a dose of 6 mg/kg doxorubicin at days indicated by the arrows. Graphs show the effects of treatment on (a) tumor growth as a function of time and (b) body weight of the animals as a measure of systemic toxicity. The top panel shows representative tumors from each treatment group. Both doxorubicin and Ful−Dox induced statistically significant tumor growth inhibition ($P < 0.05$, ANOVA). (c) Graph shows weights of excised spleen and heart following drug treatment. Inset shows representative images of heart and spleen from each treatment group. (d) Graph shows the doxorubicin distribution profiles in different organs after the animals were dosed thrice at 6 mg/kg. All data shown are mean ± SE of $n = 4−5$ per treatment group and were subjected to statistical analysis (*, $P < 0.05$; **, $P < 0.001$ ANOVA followed by Newman Keul *post hoc* test). (e) Epifluorescence images showing the effect of treatment on tumor apoptosis. Tumor sections probed for apoptosis using TUNEL assay. The cryosections were probed with fluorescent (TMR-red) terminal deoxynucleotidyl transferase-mediated dUTP nick end labeling (TUNEL) staining. Images were obtained using a Nikon Eclipse TE2000 fluorescence microscope equipped with red filter.**

liver, spleen, kidney, and tumor was quantified by fluorescence spectroscopy. Interestingly, a very high doxorubicin accumulation was observed in the spleen of the free doxorubicin treated mice (Figure 6d). This was consistent with a significant loss of spleen weight (Figure 6c), and histopathological analysis confirmed lymphocyte depletion in the periarteriolar lymphoid sheaths, with shrinkage of both the medulla and marginal zones of secondary follicles (Supporting Information, Figure 2) typical of doxorubicin-induced hematopoietic toxicity.[28,29] Furthermore, treatment with doxorubicin also resulted in significant loss of cardiac mass, consistent with cardiotoxicity reported with doxorubicin treatment.[30] Interestingly, significantly elevated levels of doxorubicin were observed in the tumor following treatment with fullerenol- or single-walled CNT-conjugated doxorubicin as compared with free doxorubicin (Figure 6d). This is consistent with the preferential passive accumulation of nanoparticles in the tumor through the EPR effect, and can explain the equieffica-ceous antitumor effect *in vivo* despite the shift in the IC_{50} *in vitro*. Furthermore, treatment with Ful−Dox induced only a minimal reduction in the weight of the spleen with no overt histopathological changes (Figure 6c and Supporting Information, Figure 2). Additionally, it exerted no cardiotoxicity as evident from the gross weight of the hearts compared with vehicle-treated group (Figure 6c). Intriguingly, we observed a significant level of doxorubicin in the lungs when administered as a CNT−Dox conjugate (Figure 6d). Furthermore, Raman spectra confirmed the presence of single-walled CNT in the lungs (see Supporting Informa-

tion, Figure 3). While single-walled CNTs have been reported to accumulate in the liver and the spleen without causing any toxicity,[31] this current observation suggests that its distribution to the lungs should be further explored. Interestingly, in contrast to the CNT−Dox, the level of doxorubicin in the lungs following administration as Ful−Dox conjugate was found to be similar to the concentration attained when administered as free doxorubicin. However, we observed elevated levels in the liver as compared with either free doxorubicin or CNT−Dox with decreased levels in the kidney, consistent with the clearance by the liver bypassing elimination by the kidney. Additionally, H&E staining of the sections of the liver indicated normal tissue pathology for the nanoparticle−doxorubicin treated group (Supporting Information, Figure 2). These results indicate that fullerenols could emerge as an exciting nanoplatform for the delivery of cytotoxics to the tumor resulting in increased therapeutic index. Furthermore, the distinctions in the tissue distribution of the carbon nanostructures *in vivo* highlight the importance of shape and size in biodistribution of nanoparticles despite identical chemical structures.

To dissect the mechanism of action, we immunostained tumor cross sections for apoptosis using TUNEL-staining, which revealed increased number of apoptotic cells inside the tumors of the animals treated with both Ful−Dox and doxorubicin (Figure 6e) as compared with animals treated with vehicle alone. The *in vivo* results were consistent with the *in vitro* observations indicating that the release of the active agent in the tumor resulted in potent apoptotic effect.

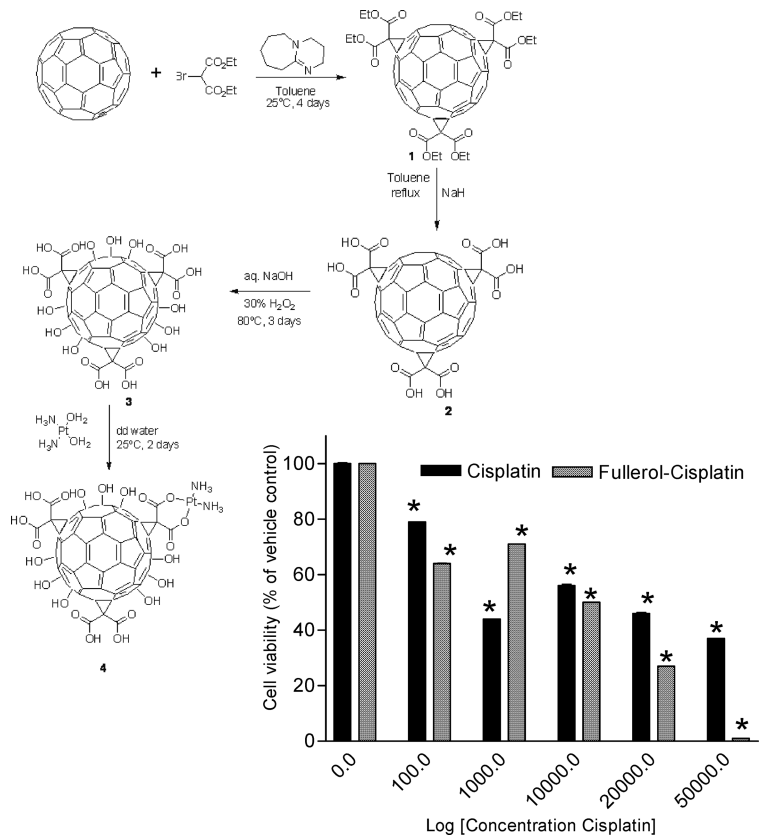

Figure 7. Synthesis and functional characterization of fullerenol−cisplatin complex. Scheme shows the synthetic steps involved in generating the fullerenol−cisplatin complex. The graph shows the concentration−effect curve of cisplatin or fullerenol−cisplatin complex on the viability of LLC cells after 48 h of incubation. Viability was measured using the MTS assay, and data was expressed as a % of vehicle-treated control. Data shown are mean ± SE of $n = 3$. Error bars were very small and are hidden within the bar. (*) $p < 0.05$ *vs* control (ANOVA followed by Newman Keuls *post hoc* test).

Extending the Fullerenol Platform to Cisplatin. As a proof of principle, to test whether the fullerenol platform can be extended to additional cytotoxics, we selected cisplatin, which is a first line chemotherapy agent for most cancers and is slightly soluble in water. Cisplatin−fullerenol complex was generated using the scheme outlined in Figure 7. Briefly, fullerene was converted into fullerene hexa-ester following treatment with diethyl malonate in dry toluene under nitrogen, to which 1,8-diazobicyclo[5,40]undec-7-ene was added. The fullerene hexaester formed was then converted into fullerene hexaacid. Fullerene hexaacid was dissolved in 1 N aqueous NaOH to which 30% H_2O_2 was added, and the resulting reaction mixture was then heated at 80 °C with continuous stirring for 3 days in open atmosphere. The reaction was allowed to cool to room temperature, and then water was removed through lyophilization to give pale red colored fullerenol hexaacid. Fullerenol hexaacid was then complexed with aquated cisplatin at room temperature for 48 h. Fullerenol hexaacid size changed from 10 nm to 30−100 nm after conjugation to cisplatin as measured using dynamic light scatter indicating that cisplatin may initiate cross-links leading to cluster formation. The final size of the fullerenol−cisplatin clusters was quantified using transmission electron microscopy and was found to be less that 100 nm. The nanoparticles were easily dispersed in deionized water and were evaluated for efficacy in a cell culture study. We selected Lewis lung carcinoma cells for the efficacy studies as cisplatin is the drug of choice for the treatment of lung cancer. As seen in Figure 7, treatment with the fullerenol−cisplatin exhibited greater antiproliferative effect on the cancer cells as compared with free cisplatin, indicating that the nanoparticles could confer an advantage to cisplatin chemotherapy. Further experiments are being conducted with the fullerenol−cisplatin conjugate and will be reported in a follow up study.

CONCLUSION

In recent years, there has been a concerted effort to integrate nanotechnology into biomedical research in order to bring radical improvements in the diagnosis, prevention, and treatment of cancer. Despite the

considerable headway made in the field of cancer nanotechnology, there is still the need to identify and develop novel nanodevices that can deliver therapeutic levels of the active agent within the tumor. This study, for the first time, demonstrates the potential application of fullerenols in cancer chemotherapy. Several components of this platform make it an attractive approach for facilitating future therapy in humans. First, the tunability of the size and the potential for increased drug loading with fullerenols can facilitate the delivery of higher concentrations of active agents to the tumor with limited entrapment in the reticuloendothelial system; in addition, the sustained release can allow a prolonged exposure of the tumor cells to the active agent. Second, the hydroxyl groups confer increased hydrophilicity, which can be useful for delivering sparingly water-soluble or hydrophobic cytotoxic agents. Finally, the multivalency of fullerenols can facilitate combination therapy from the same particle or enable the engineering of multifunctional systems that incorporate tumor homing moieties in addition to chemotherapeutics. Our study demonstrates that fullerenols can dramatically expand the repertoire of carbon nanostructures in cancer applications.

MATERIALS AND METHODS

Oxidation of Fullerene to Fullerenol. Sublimed C_{60} was purchased from Aldrich at 99.5% purity. To the fullerene (80 mg) solution in toluene (50 mL), 2 mL NaOH solution (1 g/ ml) was added followed by 5−6 drops of 30% hydrogen peroxide solution and phase transfer catalyst tetrabutyl ammoniumhydroxide (40 wt % solution in water; Aldrich). The resulting solution was stirred vigorously for 5 days at room temperature. Formation of fullerenol was indicated by high water solubility of the formed solid, which caused transfer of color from the toluene layer to the aqueous phase. The toluene layer was removed and the compound was precipitated out as a dark brown solid by addition of ethanol to the water solution. The dark solid was washed several times with ethanol to remove any excess reagent. Formation of −OH groups was evident from broad peak at 3400 cm^{-1} in FTIR.

Activation of Fullerenol. Fullerenol (60 mg) was suspended in anhydrous dimethylformamide (DMF; Sigma-Aldrich) and sonicated for 1 h to form a homogeneous suspension. To the suspension, *p*-nitrophenylchloroformate (400 mg, Sigma-Aldrich), anhydrous pyridine (2 mL), and catalytic *N*,*N*-dimethylaminopyridine (Sigma-Alrich) were added, maintaining the temperature at 0 °C. The solution was allowed to stir for 48 h, under nitrogen, along with 1 h sonication once every 8 h approximately. Product formation was indicated by increased solubility in DMF. The brown solid was precipitated out by the addition of diethyl ether and washed repeatedly with ether, dichloromethane, and isopropyl alcohol, respectively. Product was characterized by aromatic doublets at 6.9 and 8.2 ppm in proton NMR spectroscopy.

Attachment of Doxorubicin to Fullerenol. Activated fullerenol (5 mg) was dissolved in anhydrous DMF and the solution was sonicated under nitrogen for 30 min. Doxorubicin · HCl (10 mg, Tocris) was added at room temperature along with *N*,*N*-diisopropylethylamine and stirred for 10 min, after which period OMe-Peg-NH_2 (M_w = 2000, Nanocs) (half molar equivalent with respect to doxorubicin · HCl) was added. The red solution was allowed to stir at room temperature under nitrogen for 30 h along with 1 h sonication every 8 h. A red solid was precipitated out by the addition of diethyl ether. The solid was washed twice with 1−2 drops of methanol in dichloromethane. The solid was dissolved in deionized water and dialyzed for 2 days against pure water using a membrane of MWCO1000 (SpectraPor) for further purification. The solution was centrifuged at 8000 rpm for 10 min to remove bigger aggregates. The solution was lyophilized to get the required compound as a dark red solid. The presence of conjugated doxorubicin was indicated by characteristic UV−visible absorbance spectra. Dynamic light scattering and transmission electron microscopy showed the size distribution to be 50−80 nm.

For the attachment of fluorescein isothiocyanate (FITC) to fullerenol, ethylene diamine was first conjugated to FITC and then similar protocol was followed as doxorubicin attachment.

Particle Characterization. High resolution TEM images were obtained on a JEOL 2011 high contrast digital TEM. For sample preparation, lacy carbon 300 mesh copper grids (Electron Microscopy Sciences) were immersed in aqueous solutions of Ful−Dox at different concentrations, and allowed to air-dry. The size-distribution of Ful−Dox clusters was studied by dynamic light scattering (DLS), which was performed at 24 °C on a DLS-system (Malvern Zetasizer) equipped with a He−Ne laser.

Release Kinetics Studies. Concentrated drug-loaded nanoparticles were suspended in 400 μL of cell lysate and sealed in dialysis membranes (MW cutoff 1000, Spectrapor). The dialysis bags were incubated in 1.5 mL PBS buffer at room temperature with gentle shaking. A 10 μL portion of the aliquot was collected from the incubation medium at predetermined time intervals, and the released drug was quantified by absorption spectroscopy recorded on UV−vis spectrophotometer (Shimadzu UV 2450). A similar experiment was repeated in phosphate buffered saline (PBS; pH 7) to study drug release in buffer.

Cell Viability Assay. Mouse melanoma cell line B16−F10, mouse lung carcinoma (LLC1), and metastatic human breast cancer cell line MDA-MB-231 were purchased from American type Culture Collection (ATCC, Rockeville, MD). The cells were grown in Dulbecco's Modified Eagle's Medium (DMEM, Gibco) supplemented with 10% fetal bovine serum (FBS, Gibco) and antibiotics, in a humidified incubator at 37 °C (95% room air, 5% CO_2). For viability assay, the cells were grown in 96-well plates, with 2000 cells seeded into each well. When cells reached 40−50% confluency, drugs were added at appropriate concentrations (5, 10, 15 μM doxorubicin concentration). Cells were incubated in the presence of drugs at 37 °C for 24, 48, and 72 h, respectively. Cells were then washed with PBS, and MTS reagent [(3-(4,5-dimethylthiazol-2-yl)-5-(3-carboxymethoxyphenyl)-2-(4-sulfophenyl)-2*H* tetrazolium] (CellTiter 96 Aqueous One Solution Cell Proliferation Assay; Promega) was added according to the manufacturers protocol and incubated at 37 °C. Absorbance of the bioreduced soluble formazan product was measured at 490 nm using a Versamax microplate reader. Results were quantified by manually subtracting the blank value from each value then normalizing against the control values.

Cellular Uptake Studies. Cells were seeded on glass coverslips in 24-well plates, 50000 cells per well. When cells reached ~70% confluency, they were treated with fluorescein isothiocyanate (FITC)-labeled carbon nanoparticles for different durations of 30 min, 2 h, 6 h, 12 h, and 24 h, respectively. For colocalization studies, at indicated time points, the cells were washed with PBS and incubated with Lysotracker Red (Molecular Probes) at 37 °C for 30 min to allow internalization. The cells were then fixed with 4% paraformaldehyde for 20 min at room temperature, then washed twice with PBS and mounted on glass slides using Prolong Gold Antifade Reagent (Molecular Probes). Images were obtained using a Nikon Eclipse TE2000 fluorescence microscope equipped with green and red filters for FITC and Lysotracker Red, respectively.

Cell Cycle Analysis. Cells were grown in 6-well plates, 0.3×10^6 cells per well. When cells were 60−70% confluent, drugs were added in appropriate concentrations (10 μM doxorubicin concentration) and incubated for 24 h. They were then collected, treated with cold 70% ethanol, and incubated at −20 °C for 30

min to permeabilize the cell membrane. The cells were then centrifuged, washed with PBS, and resuspended in propidium iodide solution. The cell suspensions were then transferred to FACS tubes and analyzed for PI staining on a BD FACS Calibur instrument. The data was analyzed using a FloJo software.

Apoptosis Assay. Cells were grown in 6-well plates as before and incubated in the presence of nanoparticle−drug conjugate and free doxorubicin at 37 °C for 24 h. After 24 h, the cells were washed with PBS and collected at 0 °C. The cells were then treated with annexin V-Alexa Fluor 488 conjugate (Molecular Probes, Invitrogen) and incubated in the dark, at room temperature, for 15 min. The cells were then washed with PBS and incubated with propidium iodide (PI) solution (50 μg/mL; Sigma) containing RNase (1 mg/mL; Sigma). The cell suspensions were then transferred to FACS tubes and analyzed for AnnexinV/PI staining on a BD FACS Calibur instrument. Data were analyzed using a CellQuestPro software (BD Biosciences).

Murine Melanoma Model. The F10 melanoma cells (3×10^5) were implanted subcutaneously in the flanks of 4-week-old C57/BL/6 mice (weighing ≈ 20 g, Charles River Laboratories, MA). The drug therapy was started after the tumors attained volume of 50 mm^3. The tumor therapy consisted of administration of nanoparticle−doxorubicin conjugate. The formulation was prepared and validated such that 100 μL of doxorubicin−nanoparticles contained 6 mg/kg of doxorubicin (administered by tail vein injection). PBS (100 μL) administered by tail-vein injection was used as a control for drug treatment. The tumor volumes and body weights were monitored on a daily basis. The animals were sacrificed when the average tumor size of the control exceeded 10 000 mm^3. The tumors were harvested immediately following sacrifice and stored at −80 °C for further analysis. All animal procedures were approved by Harvard institutional IUCAC committee.

Doxorubicin Distribution and Histopathology. Organs (lung, heart, liver, spleen, kidney, and tumor) were weighed and cut into two halves. One half was preserved in 10% formalin for further analysis and the other half was weighed again for distribution studies. The tissue blocks were homogenized in 1% Triton X-100 solution. To 200 μL of the tissue homogenates were added 800 μL of acidified (0.75 N HCl) dichloromethane/isopropyl alcohol solution (1:1 v/v) and were kept at 4 °C for 24 h for doxorubicin extraction. Doxorubicin was measured by fluorescence at λ_{ex} = 490 nm and λ_{em} = 550 nm. The autofluorescences from the tissues were adjusted by subtracting the emission from the vehicle (PBS) treated tissues. For histopathology studies, the tissue blocks were paraffin embedded, sectioned, and stained with H&E using the core facility of Harvard Medical School.

Tumor Histology. Tumor slices (10 μm) were cut after being frozen in OCT medium and stained with standard fluorescent terminal deoxynucleotidyl transferase-mediated dUTP nick end labeling (TUNEL) staining following the manufacturer's protocol (In Situ Cell Death Detection Kit, TMR Red, Roche). Images were obtained using a Nikon Eclipse TE2000 fluorescence microscope equipped with red filter.

Synthesis and *in Vitro* Characterization of Cisplatin−Fullerenol. Cisplatin−fullerenol complex was generated through a series of steps as outlined in Figure 7. First, fullerene was converted into fullerene hexa-ester. Diethyl malonate (1.68 mL, 10 mmol) was added to a solution of fullerene (0.36 g, 0.5 mmol) in 50 mL of dry toluene in a 100 mL round-bottom flask under nitrogen, to which 1,8-diazobicyclo[5,40]undec-7-ene (1.5 mL, 10 mmol) was added. The resulting violet-colored reaction mixture was stirred at 25 °C for 96 h until the violet-colored solution turned dark red in color. Solvent was removed under vacuum and the red-colored band for C_3 and D_3 was separated. Rechromatography gave more pure major red-colored single spot (132 mg) as the product (**1**). IR v/cm^{-1} (polyethelene cassette): 2981, 2922, 2850, 2161, 1971, 1746, 1588, 1465, 1368, 1264, 1222, 1079, 1018, 855, 716, 625, 528. ^{1}H NMR (300 MHz, $CDCl_3$) δ 4.45 (q, J = 7.2 Hz, 12H), 1.37 (t, J = 7.0 Hz, 18H). ^{13}C NMR (100 MHz, $CDCl_3$) δ 163.31, 147.95, 147.34, 146.72, 146.54, 146.30, 145.33, 142.89, 142.23, 141.66, 71.0, 63.10, 51.00, 14.05.

Fullerene hexaester **1** (0.1 g) was dissolved in toluene (100 mL) to which NaH (60%, 90 mg, 2 mmol) was added, and the mixture was refluxed for 1 h. A 5 mL portion of methanol was added to this solution. The red precipitate was separated from reaction vessel by centrifugation and washed 2−3 times with toluene and hexane. The red powder was then dissolved in aqueous 4 N HCl solution. A red precipitate was formed once again, which was separated by centrifugation. Finally red solid was washed with double distilled water twice. The low molecular weight impurities are removed under vacuum to give 58 mg red−colored fullerene hexaacid (**2**). Fullerene hexaacid (**2**) (30 mg) was dissolved in 1 N aq NaOH (1 mL) to which 30 mL 30% H_2O_2 was added, and the resulting reaction mixture was then heated at 80 °C with continuous stirring for 3 days in open atmosphere. The reaction was allowed to cool to room temperature, and then water was removed through lyophilization to give 19 mg pale red-colored fullerenol hexaacid (**3**). Fullerenol hexaacid **3** (0.0015 g) was dissolved in 1 mL double distilled water containing aquated cisplatin (0.00084 g, 0.0028 mmol) in 10 mL round-bottom flask, and the resulting reaction mixture was stirred at room temperature (25 °C) for 48 h. Fullerenol hexaacid size changed from 10 nm to 30−100 nm after conjugation to cisplatin (DLS measurement). The conjugate (**4**) was further purified from unconjugated cisplatin by centrifugation. The resulting pale reddish conjugate was resuspended in double distilled water for platinum content measurement and then for further cell culture experiments. The ratio of cisplatin/fullerenol acid obtained after centrifugation using UV−vis spectroscopic method[32] was 0.89.

Statistics. All experiments were repeated independently at least thrice, and data were expressed as mean ± SE. Data were subjected to ANOVA followed by an appropriate *post hoc* test to measure statistical significance, $P < 0.05$ was set as the level of significance.

Acknowledgment. S.S. acknowledges funding from the Mary Kay Ash Foundation and the DoD BCRP Era of Hope Scholar Program (W81XWH-07-1-0482).

Supporting Information Available: Results on the cytotoxic effects of blank fullerenol nanoparticles on the different cell lines, H&E stained tissue sections of Ful-Dox, free doxorubicin and vehicle treated mice, synthesis of pegylated carbon nanotube doxorubicin conjugate and Raman signature of carbon nanotube-doxorubicin treated lung tissue. This material is available free of charge *via* the Internet at http://pubs.acs.org.

REFERENCES AND NOTES

1. US Department of Health and Human Services. National Institute of Health & National Cancer Institute. A Strategic Initiative to Transform Clinical Oncology and Basic Research Through the Directed Application of Nanotechnology. http://nano.cancer.gov/about_alliance/cancer_nanotechnology_plan.asp, July 2004.
2. Ferrari, M. Cancer Nanotechnology: Opportunities and Challenges. *Nat. Rev. Cancer* **2005**, *5*, 161–171.
3. Gabizon, A. A.; Shmeeda, H.; Zalipsky, S. Pros and Cons of the Liposome Platform in Cancer Drug Targeting. *J. Liposome Res.* **2006**, *16*, 175–183.
4. Duncan, R. The Dawning Era of Polymer Therapeutics. *Nat. Rev. Drug Discovery* **2003**, *2*, 347–360.
5. Gillies, E. R.; Frechet, J. M. J. Dendrimers and Dendritic Polymers in Drug Delivery. *Drug Discovery Today* **2005**, *10*, 35–43.
6. Geng, Y.; Dalhaimer, P.; Cai, S.; Tsai, R.; Tewari, M.; Minko, T.; Discher, D. E. Shape Effects of Filaments *versus* Spherical Particles in Flow and Drug Delivery. *Nat. Nanotechnol.* **2007**, *2*, 249–255.
7. Nakamura, E.; Isobe, H. Functionalized Fullerenes in Water. The First 10 Years of Their Chemistry, Biology, and Nanoscience. *Acc. Chem. Res.* **2003**, *36*, 807–815.
8. Liu, Z.; Chen, K.; Davis, C.; Sherlock, S.; Cao, Q.; Chen, X.; Dai, H. Drug Delivery with Carbon Nanotube for *in Vivo* Cancer Treatment. *Cancer Res.* **2008**, *68*, 6652–6660.
9. Zerda, A. D. L.; Zavaleta, C.; Karen, S.; Vaithilingam, S.; Bodapati, S.; Liu, Z.; Levi, J.; Smith, B. R.; Ma, T. -J.; Oralkan, O.; Chang, Z.; Chen, X.; Dai, H.; Khuri-Yakub, B. T.; Gambhir,

S. S. Carbon Nanotubes as Photoacoustic Molecular Imaging Agents in Living Mice. *Nat. Nanotechnol.* **2008**, *3*, 557–562.
10. Foley, S.; Crowley, C.; Smaihi, M.; Bonfils, C.; Erlanger, B. F.; Seta, P.; Larroque, C. Cellular Localization of a Water-Soluble Fullerene Derivative. *Biochem. Biophys. Res. Commun.* **2002**, *294*, 116–119.
11. Bakry, R.; Vallant, R. M.; Najam-ul-Haq, M.; Rainer, M.; Szabo, Z.; Huck, C. W.; Bonn, G. K. Medical Applications of Fullerenes. *Int. J. Nanomed.* **2007**, *2*, 639–649.
12. Isobe, H.; Nakanishi, W.; Tomita, N.; Jinno, S.; Okayama, H.; Nakamura, E. Nonviral Gene Delivery by Tetraamino Fullerene. *Mol. Pharm.* **2006**, *3*, 124–134.
13. Marchesan, S.; Da Ros, T.; Spalluto, G.; Balzarini, J.; Prato, M. Anti-HIV Properties of Cationic Fullerene Derivatives. *Bioorg. Med. Chem.* **2005**, *15*, 3615–3618.
14. Mroz, P.; Tegos, G. P.; Gali, H.; Wharton, T.; Sarna, T.; Hamblin, M. R. Photodynamic Therapy with Fullerenes. *Photochem. Photobiol. Sci.* **2007**, *6*, 1139–149.
15. Ali, S. S.; Hardt, J. I.; Quick, K. L.; Kim-Han, J. S.; Erlanger, B. F.; Huang, T. T.; Epstein, C. J.; Dugan, L. L. A Biologically Effective Fullerene (C_{60}) Derivative with Superoxide Dismutase Mimetic Properties. *Free Radical Biol. Med.* **2004**, *37*, 1191–1202.
16. Wharton, T.; Wilson, L. J. Highly-Iodinated Fullerene as a Contrast Agent for X-ray Imaging. *Bioorg. Med. Chem.* **2002**, *10*, 3545–3554.
17. Cagle, D. W.; Kennel, S. J.; Mirzadeh, S.; Alford, J. M.; Wilson, L. J. *In Vivo* Studies of Fullerene-Based Materials Using Endohedral Metallofullerene Radiotracers. *Proc. Natl. Acad. Sci. U.S.A.* **1999**, *96*, 5182–5187.
18. Mikawa, M.; Kato, H.; Okumura, M.; Narazaki, M.; Kanawaza, Y.; Miwa, N.; Shinohara, H. Paramagnetic Water-Soluble Metallofullerenes Having the Highest Relaxivity for MRI Contrast Agents. *Bioconjugate Chem.* **2001**, *12*, 510–514.
19. Ashcroft, J. M.; Tsyboulski, D. A.; Hartman, K. B.; Zakharian, T. Y.; Marks, J. W.; Weiman, R. B.; Rosenblum, M. G.; Wilson, L. J. Fullerene (C_{60}) Immunoconjugtes: Interaction of Water-Soluble C_{60} Derivatives with the Murine Anti-gp240 Melanoma Antibody. *Chem. Commun.* **2006**, 3004–3006.
20. Zakharian, T. Y.; Seryshev, A.; Sitharaman, B.; Gilbert, B. E.; Knight, V.; Wilson, L. J. A Fullerene-Paclitaxel Chemotherapeutic: Synthesis, Characterization, and Study of Biological Activity in Tissue Culture. *J. Am. Chem. Soc.* **2005**, *127*, 12508–12509.
21. Partha, R.; Mitchell, L. R.; Lyon, J. L.; Joshi, P. P.; Conyers, J. L. Buckysomes: Fullerene-Based Nanocarriers for Hydrophobic Molecule Delivery. *ACS Nano* **2008**, *2*, 1950–1958.
22. Kokubo, K.; Matsubayashi, K.; Tategaki, H.; Takada, H.; Oshima, T. Facile Synthesis of Highly Water-Soluble Fullerenes More Than Half-Covered by Hydroxyl Groups. *ACS Nano* **2007**, *2*, 327–333.
23. Peer, D.; Karp, J. M.; Hong, S.; Farokhzad, O. C.; Margalit, R.; Langer, R. Nanocarriers as an Emerging Platform for Cancer Therapy. *Nat. Nanotechnol.* **2007**, *2*, 751–760.
24. Basu, S.; Harfouche, R.; Soni, S.; Chimote, G.; Mashelkar, R. A.; Sengupta, S. Nanoparticle-Mediated Targeting of MAPK Signaling Predisposes Tumor to Chemotherapy. *Proc. Natl. Acad. Sci. U.S.A.* **2009**, *106*, 7957–7961.
25. Ruoslahti, E.; Duza, T.; Zhang, L. Vascular Homing Peptides with Cell-Penetrating Properties. *Curr. Pharm. Des.* **2005**, *11*, 3655–3660.
26. Xu, G.; Zhang, W.; Ma, M. K.; McLeod, H. Z. Human Carboxylesterase2 Is Commonly Expressed in Tumor Tissue and Is Correlated with Activation of Irinotecan. *Clin. Cancer. Res.* **2002**, *8*, 2605–2611.
27. Devi, L.; De Grot, F. M. H.; Blacher, S.; Hajitou, A.; Beusker, P. H.; Scheeren, H. W.; Foidart, J. -M.; Noel, A. Plasmin-Activated Doxorubicin Prodrugs Containing a Spacer Reduce Tumor Growth and Angiogenesis Without Systemic Toxicity. *FASEB J.* **2004**, *18*, 564–567.
28. OKunewick, J. P.; Buffo, M. J.; Kociban, D. L. Comparative Toxicity of Mitoxantrone and Doxorubicin on Hematopoietic Stem Cells. *Exp. Hematol.* **1985**, *13*, 23–30.
29. Ruchatz, H.; Puttini, M.; Cleris, L.; Pilotti, S.; Gambacorti-Passerini, C.; Formelli, F. Effect of Imatinib on Haematopoietic Recovery Following Idarubicin Exposure. *Leukemia* **2003**, *17*, 298–304.
30. Hamed, S.; Barshack, I.; Luboshits, G.; Wexler, D.; Deutsch, V.; Keren, G.; George, J. Erythropoietin Improves Myocardial Performance in Doxorubicin-Induced Cardiomyopathy. *Eur. Heart J.* **2006**, *27*, 1876–1883.
31. Schipper, M. L.; Nakayama-Ratchford, N.; Davis, C. R.; Kam, N. W.; Chu, P.; Liu, Z.; Sun, X.; Dai, H.; Gambhir, S. S. A Pilot Toxicology Study of Single-Walled Carbon Nanotubes in a Small Sample of Mice. *Nat Nanotechnol.* **2008**, *3*, 216–221.
32. Scheechter, B.; Pauzner, R.; Arnon, R.; Wilchek, M. Cis-platinum(II) Complexes of Carboxymethyl−Dextran as Potential Antitumor Agents I. Preparation and Characterization. *Cancer Biochem. Biophys.* **1986**, *8*, 277–287.